# Facile synthesis and photoluminescence mechanism of graphene quantum dots

Ping Yang,[1] Ligang Zhou,[1] Shenli Zhang,[1] Neng Wan,[2] Wei Pan,[1,a)] and Wenzhong Shen[1,b)]

[1]*Laboratory of Condensed Matter Spectroscopy and Opto-Electronic Physics, and Key Laboratory of Artificial Structures and Quantum Control (Ministry of Education), Department of Physics and Astronomy, Shanghai Jiao Tong University, Shanghai 200240, China*
[2]*SEU-FEI Nano Pico Center, Key Laboratory of MEMS of Ministry of Education, School of Electronics Science and Engineering, Southeast University, Nanjing 210096, China*

We report a facile hydrothermal synthesis of intrinsic fluorescent graphene quantum dots (GQDs) with two-dimensional morphology. This synthesis uses glucose, concentrate sulfuric acid, and deionized water as reagents. Concentrated sulfuric acid is found to play a key role in controlling the transformation of as-prepared hydrothermal products from amorphous carbon nanodots to well-crystallized GQDs. These GQDs show typical absorption characteristic for graphene, and have nearly excitation-independent ultraviolet and blue intrinsic emissions. Temperature-dependent PL measurements have demonstrated strong electron-electron scattering and electron-phonon interactions, suggesting a similar temperature behavior of GQDs to inorganic semiconductor quantum dots. According to optical studies, the ultraviolet emission is found to originate from the recombination of electron-hole pairs localized in the C=C bonds, while the blue emission is from the electron transition of $sp^2$ domains. © 2014 AIP Publishing LLC. [http://dx.doi.org/10.1063/1.4904958]

## I. INTRODUCTION

Graphene, a monolayer of $sp^2$-bonded carbon atoms, has attracted great attention due to its distinctive properties,[1–4] such as superior mechanical flexibility, high intrinsic mobility, excellent thermal/chemical stability, and environmentally friendly nature, leading to wide applications on electronic devices. Despite the above-mentioned unique properties, as intrinsic graphene is a zero-bandgap material, the observation of its luminescence is almost impossible, which impedes its application in optoelectronics.[5,6] Theoretical studies have predicted that graphene has pronounced quantum confinement effect and its bandgap can be tuned from 0 eV to that of benzene by varying the size.[7–10] Consequently, to expand the application area of graphene to optical-related field, one promising approach is to convert the graphene into graphene quantum dots (GQDs).[11]

In the past few years, many efforts have been paid in the synthesis and fabrication of fluorescent GQDs by organic synthesis starting from small molecules and approaches ranging from simple oxidation to cutting carbon sources.[11–27] These GQDs by various methods can emit luminescence with different colors from deep ultraviolet to near-infrared region. However, most GQDs were partially oxidized quantum dots, and the oxygen-containing functional groups on the surfaces introduce a series of emissive traps into the $\pi$-$\pi$* gap.[12–15] The couple of defect state emission to intrinsic state emission from differently sized GQDs makes GQDs prepared by various methods exhibit different photoluminescence (PL) mechanisms,[12] including quantum confinement effect,[16,17] zigzag edge sites,[18–20] or recombination of localized electron-hole

pairs.[21,22] Recent experimental studies[13–15] have pointed out that the green emission in graphene oxide quantum dots (GOQDs) is closely related to O functional groups, while the blue luminescence in reduced GOQDs and *pure* GQDs is derived from intrinsic state emission. However, the detailed PL mechanism inside the *pure* GQDs is still unclear. Further studies should be carried out to explore it because PL mechanism is crucial to the understanding and modulation of GQDs in opto-electronic properties.

Here, we use a facile hydrothermal method to synthesize intrinsic fluorescent GQDs by using glucose, concentrate sulfuric acid, and deionized water as reagents. The well-crystallized intrinsic GQDs with a quantum yield (QY) of 17% were obtained by controlling the sulfuric acid and reaction temperature. These GQDs with high quality exhibit sharp band-edge absorption, typical excitonic absorption peak, and nearly excitation-independent ultraviolet and blue intrinsic emissions. Optical characterization indicates the ultraviolet emission is from the recombination of electron-hole pairs localized in the C=C bonds, while the blue originates from electron transition of $sp^2$ domains. Temperature-dependent photoluminescence measurements further demonstrate the existence of strong electron-phonon and electron-electron interaction, suggesting a similar temperature behavior of GQDs to inorganic semiconductor quantum dots. The results provide a further understanding of PL mechanism in GQDs, and are helpful to promote their applications on optoelectronic devices, such as solar cell and photodetector.

## II. EXPERIMENTAL DETAILS

The GQDs were prepared by a hydrothermal method by using glucose, concentrate sulfuric acid ($H_2SO_4$), and deionized water as precursors. In a typical synthesis, 1.5 g of

a)E-mail: sjtushelwill@sjtu.edu.cn
b)E-mail: wzshen@sjtu.edu.cn

glucose was dissolved in 10 ml of deionized water, followed by the introduction of 10 ml of $H_2SO_4$. The mixture was then treated by a one-step hydrothermal method in Teflon-lined stainless-steel autoclave (50 ml) at 200 °C for 3 h, producing GQDs dispersions with good solubility in water after filtration with the qualitative filter paper (15–20 $\mu$m particle retention). The samples were neutralized with sodium hydroxide for further characterization.

The morphologies and dimensions of GQDs were revealed by using a Titan 80–300 transmission electron microscopy (TEM) with an accelerating voltage of 200 kV. Atomic force microscope (AFM) images were measured by using a Seiko Nanonavi E-Sweep AFM. X-ray diffraction (XRD) patterns were recorded by a Rigaku SmartLab X-ray diffractometer with a Cu K$\alpha$ radiation source. X-ray photoelectron spectroscopy (XPS) experiments were performed using a PHI Quantum 2000 XPS system with a monochromatic Al K$\alpha$ X-ray source. Fourier transform infrared

(FT-IR) spectra were performed by using a Bruker Vertex 70 FT-IR spectrometer. Raman and temperature-dependent PL spectra were obtained by a Jobin Yvon LabRAM HR 800 UV micro-Raman spectrometer system. UV-vis absorption and excitation-dependent PL spectra were measured on a Perkin-Elmer Lambda 20 UV/Vis spectrometer and a Perkin Elmer LS 50B luminescence spectrometer, respectively. The QY of GQDs was obtained in reference to quinine sulfate.

## III. RESULTS AND DISCUSSIONS

In the early stages, the hydrothermal treatment of carbohydrates generally produces the amorphous carbon nanodots. Tang et al.[23] have realized the synthesis of spherical GQDs by combining the microwave technique and hydrothermal method. Recently, Li et al.[24] have reported the hydrothermal synthesis of S-doped spherical GQDs in $H_2SO_4$ environment and studied the effect of sulphur doping on the electronic
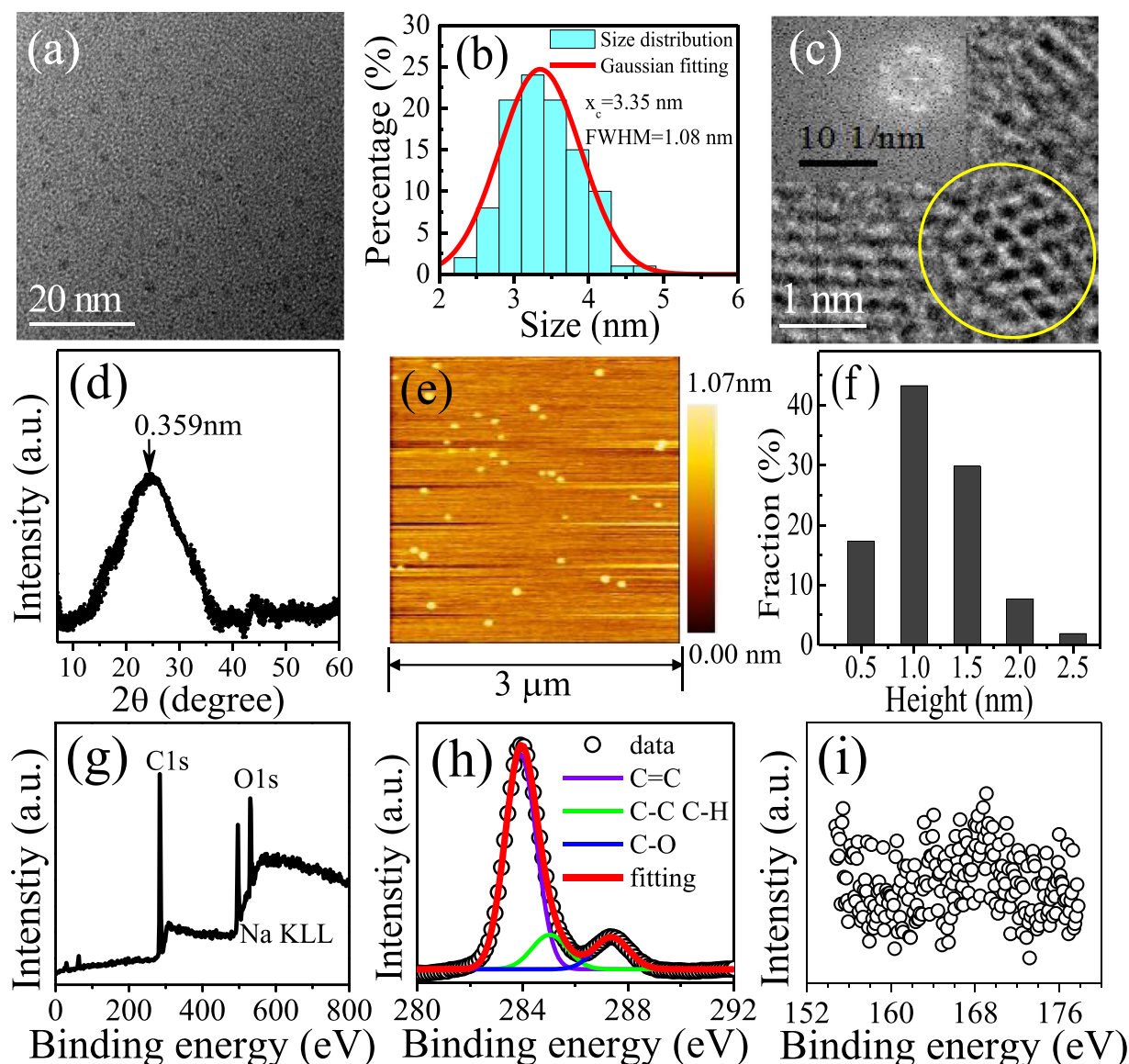


FIG. 1. (a) TEM image of the GQDs on copper grid coated with ultrathin amorphous carbon film; (b) size distribution of GQDs with the Gaussian fitting (red curve); (c) HRTEM image of a typical GQD. The inset is the corresponding selected area FFT image; (d) XRD spectrum of GQDs assembled on the silicon substrate; (e) AFM image of GQDs; (f) height profile of the GQDs; (g) the full-scan XPS spectrum of GQDs; (h) the C1s XPS; and (i) the S2p XPS spectra of the GQDs.

structure and optical properties. Here, we have realized the hydrothermal synthesis of intrinsic and highly crystallized fluorescent GQDs with 2D morphology in ionic solutions (with water existence).

Fig. 1(a) displays the TEM of GQDs synthesized at 200 °C with 10 ml of $H_2SO_4$ and 10 ml of deionized water. Statistical analysis of TEM image gives a Gaussian size distribution in Fig. 1(b), which locates at 3.35 nm with a full width at half maximum (FWHM) of 1.08 nm, representing a narrow size distribution. The typical high-resolution TEM (HRTEM) image shown in Fig. 1(c) exhibits the high crystallinity of GQDs. The in-plane lattice spacing of GQDs (yellow circle) is 0.244 nm, calculated from the corresponding selected area of fast Fourier transform image [see inset of Fig. 1(c)]. This value is very close to that (0.250 nm) of graphene,[9,28] indicating the graphitic structure of the GQDs. The average distance between the C−C bonds is 1.408 ± 0.012 Å, in good agreement with numerical values[29] and other experimental results of GQDs.[30] XRD spectrum in Fig. 1(d) shows a wide (002) diffraction peak at 24.80°, corresponding to a graphitic structure.[19,20] The interlayer spacing of 0.359 nm calculated from XRD agrees well with previously reported values (0.340–0.403 nm) of GQDs,[12] and slightly higher than the value (0.34 nm) of bulk graphite. Both the in-plane and basal lattice parameters indicate that the GQDs exhibit the graphitic structure, not the diamond one. AFM image in Fig. 1(e) and the height profile in Fig. 1(f) display the height distribution of GQDs, which demonstrate that most of the GQDs are composed of two

graphene layers, indicating GQDs have a disk shape, not a spherical one. XPSs in Figs. 1(g)–1(i) are performed to determine the composition of the GQDs. The full-scan XPS spectrum in Fig. 1(g) clearly displays the C1s (∼284 eV) and O1s (∼532 eV) signals. The high-resolution C1s XPS spectrum in Fig. 1(h) reflects the existence of C=C (284.0 eV), C−C/C−H (285.0 eV), and C−O−C (287.4 eV). The dominant C=C component suggests that C=C bonds is the elementary unit in the GQDs. The high-resolution S2p XPS spectrum in Fig. 1(i) shows the weak and random signal, suggesting no detectable presence of C−S bond in the GQDs. It indicates our GQDs are actually intrinsic, not as S-doped GQDs fabricated by Li *et al.*[24] The composition of the GQDs is also confirmed by FTIR spectrum (see Fig. S1 in Ref. 31), which displays the presence of C=C (∼1550 cm$^{-1}$), C−H (∼1431 cm$^{-1}$), the C−O (∼1130 cm$^{-1}$), and O−H (band at ∼3400 cm$^{-1}$) peaks of $H_2O$.

The above observation exhibits the good crystallinity of our GQDs, which is probably induced by $H_2SO_4$ ionic solution. To clarify it, we investigate the structural characteristics of B0–200, B2–200, B5–200, and B10–200, which are synthesized at a fixed temperature of 200 °C, with different $H_2O:H_2SO_4$ (vol:vol) of 20:0 ml, 18:2 ml, 15:5 ml, and 10:10 ml, respectively. HRTEM images in Figs. 2(a)–2(d) demonstrate that the as-products (B0–200) synthesized without $H_2SO_4$ is amorphous. The addition of $H_2SO_4$ realizes the amorphous-to-crystalline transformation. With the increase of $H_2SO_4$, the crystallinity of nanoparticles is obviously improved, as shown in Figs. 2(d) and S2.[31] Fig. 2(e) displays
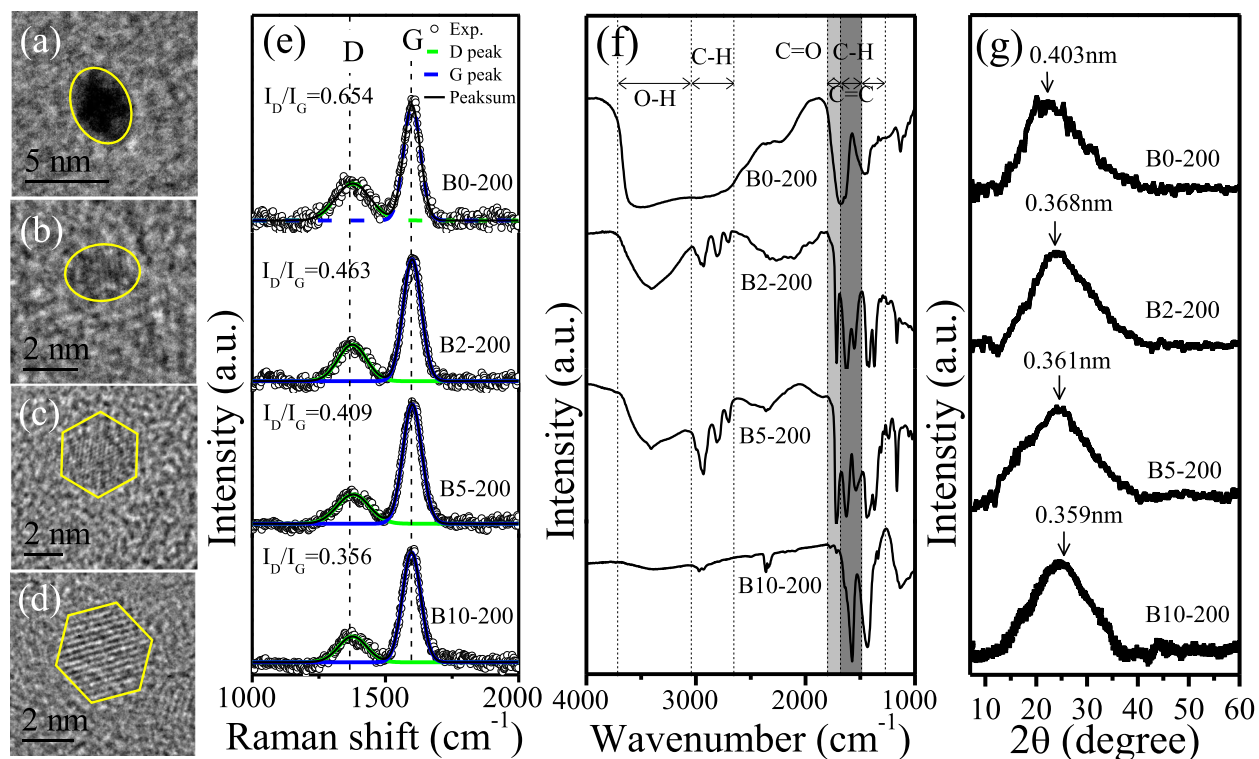


FIG. 2. HRTEM images of (a) B0-200, (b) B2-200, (c) B5-200, and (d) B10-200; (e) Raman spectra, (f) FT-IR spectra, and (g) XRD spectra of B0-200 (up), B2-200 (second), B5-200 (third), and B10-200 (bottom).

the Raman spectra of B0–200, B2–200, B5–200, and B10–200, with an excitation wavelength of 325 nm after baseline correction to exclude the influence of fluorescence. Typical D-($\sim$1380 cm$^{-1}$) and G-band ($\sim$1600 cm$^{-1}$) are observed in all of the four samples. The G-band is related to the $E_{2g}$ mode of all pairs of $sp^2$ atoms both in rings and chains, corresponding to the in-plane vibrations of the graphitic structure, while the D-band comes from the transverse optical (TO) phonon around K-point of the Brillouin zone and requires a defect for its activation.[32,33] The intensity ratio of D-band to G-band ($I_D/I_G$) in Fig. 2(e) is found to decrease with the increasing H$_2$SO$_4$, proving the fact that H$_2$SO$_4$ can decrease the defects in the GQDs and improve their quality.

Fig. 2(f) presents the FT-IR spectra of B0–200, B2–200, B5–200, and B10–200, from which we can investigate the bonding composition and functional groups. The FT-IR spectrum of B0–200 shows a strong absorption band at 3400 cm$^{-1}$ due to O$-$H, and absorption peaks at 1678 cm$^{-1}$ due to C=O and around $\sim$1639 cm$^{-1}$ induced by aromatic C=C stretching. Considering the random dehydration of glucose without H$_2$SO$_4$, disordered arrangement of carbon structure may probably be formed in the B0–200. With H$_2$SO$_4$, besides the aromatic C=C stretching band ($\sim$1630 cm$^{-1}$), a new absorption peak at 1550 cm$^{-1}$ is observed, which reflects the C=C conjugation vibration frequently observed in graphene.[19,34] With the increase of H$_2$SO$_4$, the C=C conjugation vibration is obviously enhanced, while the bands due to aromatic C=C ($\sim$1630 cm$^{-1}$), C=O ($\sim$1715 cm$^{-1}$), and C$-$H ($\sim$2925, $\sim$2807, and 2700 cm$^{-1}$) groups are gradually weakened. The existence of C=C conjugated vibration rather than aromatic C=C vibration (generally located at $\sim$1630 cm$^{-1}$) indicates the formation of ordered carbon backbone structure. The weakening of the vibration due to C=O, O$-$H, and C$-$H groups illustrates the decrease of O functional groups decorated on the carbon backbone structure. Apparently, due to the existence of H$_2$SO$_4$, the O and H atoms are gradually stripped off from the C$-$OH, C$-$H, and C=O groups, forming the carbon backbone with a non-uniform coverage of O functional groups. These groups will remain in the GQDs unless there is enough H$_2$SO$_4$ to completely remove them from the carbon backbone. The role of H$_2$SO$_4$ on removing O functional groups can be observed from XRD spectra of B0–200, B2–200, B5–200, and B10–200 shown in Fig. 2(g). It clearly demonstrates the decrease of interlayer spacing with the increase of the H$_2$SO$_4$.

Since the O functional groups in the GQDs generally result in the defect states,[12–15] the elimination of O functional groups reduces the defect states and then weakens the corresponding band-tail absorption (see Fig. S3 in Ref. 31). Furthermore, with the decrease of defects states and the improvement of crystallinity, the QY increases from 0.99% to 14.3%, and PL spectra exhibit different dependence on excitation wavelength ($\lambda_{ex}$) (see Fig. S4 in Ref. 31). The PL spectra of B0–200, B2–200, and B5–200 samples show the obvious $\lambda_{ex}$-dependent green emission over a wide range of $\lambda_{ex}$, which demonstrate the dominant contribution of defect state emission due to the wide distributed defect energy

levels.[12,13] With the enhancement of crystallinity, defect state emission becomes weak and intrinsic state emission increases, so that nearly $\lambda_{ex}$-independent blue emission is observed in B10–200 with $\lambda_{ex}$ of 320–400 nm. Similar results were also observed from the GQDs grown with 10 ml of H$_2$SO$_4$ and 10 ml of deionized water at different reaction temperatures (160, 180, 200, and 220 °C). These GQDs can emit brightly nearly $\lambda_{ex}$-independent blue fluorescence with QYs of 8%–17% (see Figs. S5 and S6 in Ref. 31). FT-IR spectra (see Fig. S5(a) in Ref. 31) clearly display the conjugated C=C vibration peak at $\sim$1550 cm$^{-1}$, indicating the formation of ordered carbon backbone in GQDs. The gradually weakened C=O vibration peaks, as well as the decreasing band-tail absorption (see Fig. S5 in Ref. 31), illustrate that the crystallinity of GQDs is enhanced with the increase of reaction temperature. Moreover, their QYs are enhanced with the increasing reaction temperature (see Fig. S5 in Ref. 31). The variation of QY with crystallinity indicates that the blue emission of GQDs probably comes from the intrinsic state emission, not the defect state one.

To explore the PL origin of GQDs in details, we chose the best GQDs (B10–220) synthesized at 220 °C with 10 ml of H$_2$SO$_4$ and 10 ml of deionized water as a platform to investigate their optical properties. Fig. 3(a) displays the UV-vis absorption, PL, and PL excitation (PLE) spectra of GQDs aqueous solution measured with Xenon and Deuterium lamps. The absorption spectrum of GQDs (red line) displays a significant absorption edge and two absorption peaks at 275 and 205 nm, respectively. The distinct absorption peak at 275 nm is attributed to the electron transition of $sp^2$ carbon domains, for its transition energy (4.51 eV) is consistent with that of 4.59 eV in the graphene sheets from UV-vis absorption spectra [30] and that of 4.50 eV in bilayer graphene structure from first-principles calculation.[35] The existence of this peak suggests the formation of delocalized $\pi$ states on the basal plane like those in graphene. The peak at 205 nm is assigned to the $\pi \rightarrow \pi^*$ transition of C–C bonds after considering that the $\pi \rightarrow \pi^*$ transition of aromatic C–C bonds in GQDs is commonly located at a wavelength between 200–270 nm.[12]

On excitation at 205 nm, GQDs exhibit dual emissions [green line in Fig. 3(a)], a strong blue emission ($\sim$419 nm), and a weak ultraviolet one ($\sim$311 nm). The PLE spectrum detected at 420 nm [blue line in Fig. 3(a)] shows a distinct peak at 357 nm and a small peak at 240 nm, corresponding to the absorption peaks at 275 and 205 nm, respectively. Due to the experimental limit, it is hard to identify the peak position of PLE spectrum detected at 311 nm. However, from the $\lambda_{ex}$-dependent PL spectra in Fig. 3(b), it is found that the PLE peak is probably around 210 nm, which corresponds to the absorption peak at 205 nm. Therefore, this ultraviolet emission is assigned to the transition of $\pi$ electrons localized in C–C bonds, in consistence with the previous reports.[23,36] The simultaneously observed blue fluorescence in our GQDs [Fig. 3(c)] is found to be nearly irrespective of $\lambda_{ex}$ when excited by a series of monochromatic light with $\lambda_{ex}$ of 300–360 nm, opposite to the $\lambda_{ex}$-dependent characteristics of defect state emission. Here, using $\lambda_{ex}$ of 300–360 nm to emit blue fluorescence is to eliminate the interference of
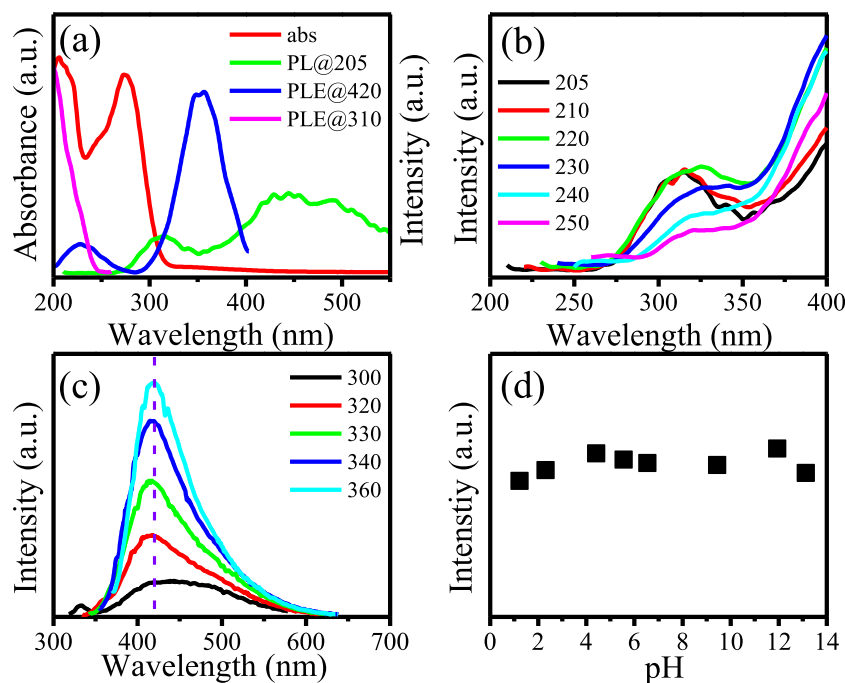
FIG. 3. (a) UV-vis absorption (Abs, red), PL (at 205 nm excitation, green), PLE (at 420 nm emission, blue) and PLE (at 310 nm emission, magenta) spectra of GQDs; (b) PL spectra excited at 205–250 nm excitation; (c) PL spectra excited at 300–360 nm excitation; (d) PL intensity at different pH.

second-order diffraction light of excitation source (see Fig. S7 in Ref. 31). Furthermore, the blue emission is stable against the pH variation of the solutions from strong acid to base [Fig. 3(d)] in contrast to the strongly pH-dependent PL of free zigzag edge sites.[18,19] Considering the above optical properties, the blue fluorescence is temporarily assigned to the π electron transition of $sp^2$ carbon domains.

To get an insight of the PL mechanism of GQDs, we have also carried out the temperature-dependent PL measurements from 80 to 300 K. Compared with the room temperature PL measurements, the temperature-dependent PL may offer more useful information about the PL mechanism. The temperature-dependent peak energy, linewidth, and intensity are helpful to understand the nature of radiative transition.[37–44] To perform the measurements, concentrated GQDs dispersions are drop-casted on the intrinsic silicon wafer, followed by heating at 120 °C for 10 min to dry it in nitrogen atmosphere.

Fig. 4(a) shows the PL spectra of GQDs thin film excited by 325 nm laser at five typical temperatures of 83, 133, 183, 233, and 293 K. Similar to those observed in the GQDs aqueous solution, each PL spectrum of GQDs thin film displays two PL peaks, located at ∼3.25 eV (peak A) and ∼2.54 eV (peak B), respectively. The variation of PL peaks with temperature is given in Fig. 4(b). As shown in this figure, with the increasing temperature, peak A displays a blueshift of ∼80 meV, but peak B exhibits a redshift of ∼100 meV. This blueshift behavior is commonly observed from the temperature-dependent radiative transition of π electrons localized at C–C bonds in conjugated polymer with a distribution of chain lengths.[38–40] With the increasing temperature, the created excitons produced by localized π electrons transition do not easily migrate to the low energy segments, and remain localized on the shorter chain segments with higher energies,[40] finally leading to the blueshift of PL peak with the increasing temperature. Therefore, the

peak A is thought to be from the transition of π electrons localized at C–C bonds, in agreement with the former conclusion. The redshift phenomenon of peak B is similar to the bandgap shrinkage of inorganic semiconductors,[40–42]
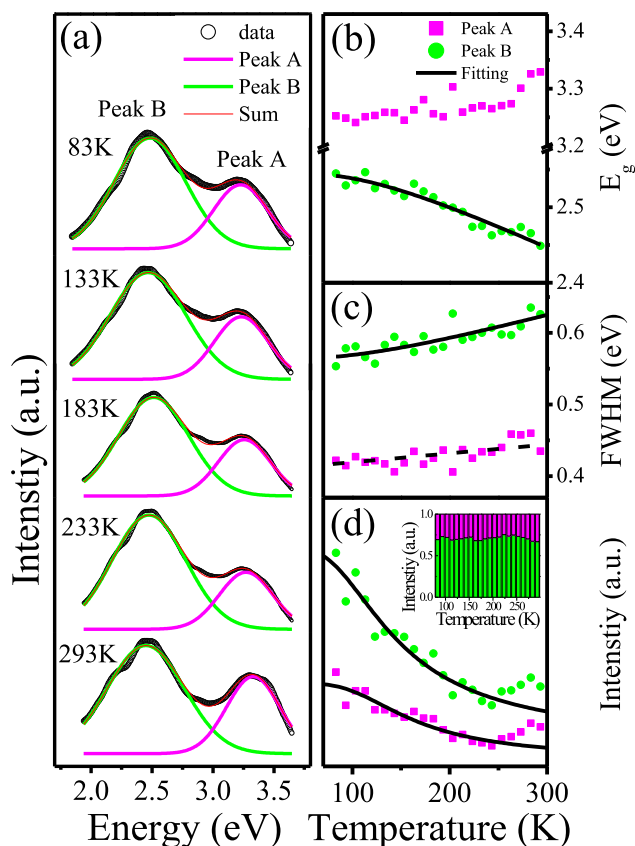


FIG. 4. (a) PL spectra of GQDs at five typical temperatures. Two emissions around 3.25 eV and 2.54 eV are denoted as peak A (magenta) and peak B (green), respectively. Temperature-dependent (b) emission peak, (c) FWHM, and (d) integrated PL intensity. The inset of (d) is histogram of temperature-dependent intensity weight of peaks A and B.

suggesting the interband-like transition of peak B. Consequently, an expression proposed by O'Donnell and Chen[43] is used to fit the experimental results, which is based on the analysis of the electron-phonon coupling mechanism responsible for the band gap shift

$$E_g(T) = E_g(0) - 2SE_{ph}/[\exp(E_{ph}/k_BT) - 1], \quad (1)$$

where $E_g(0)$ is the transition energy at $0\,K$, $S$ is the Huang-Rhys factor, representing the strength of the electron-phonon coupling, and $E_{ph}$ is the average phonon energy. The best fit for peak B yields the parameters $E_g(0) = 2.544 \pm 0.008$ eV, $E_{ph} = 32.56 \pm 1.16$ meV, and $S = 3.67 \pm 0.87$. The $S$ is larger than not only [$(3.98 \pm 0.37) \times 10^{-4}$] in carbon nanodots,[44] but also those in CdSe/CdS dot-in-rods nanocrystals (1.57)[41] and InP/ZnS core-shell quantum dots (1.64–3.02),[42] representing a stronger electron-phonon coupling.

Fig. 4(c) shows the relationship between FWHM and temperature. From this figure, it is found that the FWHM of peak A almost remains constant and that of peak B increases with the temperature. Previous studies[41,42,44] have shown that the total FWHM can be described by a temperature-independent intrinsic term $\Gamma_0(0)$ (dominantly electron-electron scattering), temperature-dependent electron-acoustic phonon scattering $\gamma_{AC}T$, and electron-LO phonon scattering $\Gamma_{LO}/[\exp(E_{LO}/k_BT)-1]$ term. The large FWHMs of peak A (400 meV) and peak B (550 meV) at low temperature (83 K) indicate the existence of strong electron-electron interaction. The variation of bandwidth of peak B suggests the existence of electron-phonon interaction, so that we use the formula $\Gamma_0(0) + \gamma_{AC}T + \Gamma_{LO}/[\exp(E_{LO}/k_BT)-1]$ to fit it. A good agreement between the experimental data and the best-fit curve is obtained for $\Gamma_0(0) = 0.562$ eV, $\gamma_{AC} = 0.427$ meV K$^{-1}$, $E_{LO} = 32.56$ meV, and $\Gamma_{LO} = 127$ meV. These relative large coefficients suggest the existence of strong electron-electron scattering and electron-phonon interaction, in consistence with the above conclusion from the variation of peak energy with temperature. It is worth noting that in graphene, the electron-phonon coupling is so strong that results in the renormalization of electron bands.[45] This implies that the blue emission in GQDs indeed comes from electron transition of $sp^2$ domains, and the distinct redshift of PL peak with increasing temperature is from the electron bands renormalization induced by strong electron-phonon interactions.

Fig. 4(d) shows the temperature-dependent integrated PL intensity of peaks A and B. From this figure, it is observed that below 240 K the PL intensity of these two peaks simultaneously decreases with the increasing temperature, indicating a thermally activated process is involved in the carrier relaxation. At low temperatures, the nonradiative channel is not thermally activated, and become thermally activated once the temperature increases, as expressed by $\tau_{nr} = \tau_0\exp(E_a/k_BT)$, where $E_a$ is the activation energy. The nonradiative lifetime $\tau_{nr}$ decreases with the increasing temperature, leading to a decrease of PL intensity, which can be described as the following equation:[41,44]

$$I(T) = I_0/[1 + (\tau_r/\tau_0) \times \exp(-E_a/k_BT)], \quad (2)$$

where $I_0$ and $I(T)$ are the PL intensity at $0\,K$ and any given temperature, $\tau_r$ and $\tau_0$ are the radiative and nonradiative lifetime, respectively. Fig. 4(d) also displays the best fitting results for peak A and peak B. The activation energy is 45.4 (peak A) and 34.5 meV (peak B), while lifetime ratio ($\tau_r/\tau_0$) is 20.2 (peak A) and 11.3 (peak B). These relatively higher activation energies suggest a low density of defect states, which are probably induced by the inevitable vacancy and interstitial atoms. Moreover, based on the values of $\tau_r/\tau_0$ and $E_a$, the quantum efficiency of GQDs can be estimated from the formula $\eta = 1/[1 + \tau_r/\tau_0\exp(-E_a/k_BT)]$. The quantum efficiency of blue emission at room temperature is calculated to be 22%, close to the result of 17% directly measured with quinine sulfate as standard. In addition, it is found that the PL intensity ratio of peak A to peak B remains constant at various temperatures [inset of Fig. 4(d)], indicating the two radiative transitions are not competitive with each other. Actually, the photoexcited electrons would be either relaxed into $sp^2$ domains or localized at C–C bonds accompanied with the vibration relaxation, and produce excitation-independent blue and ultraviolet emissions, respectively.

## IV. CONCLUSIONS

In summary, we have used a facile hydrothermal method to synthesize intrinsic fluorescent GQDs with QY of 17%. By using the glucose, sulfuric acid, and deionized water, it is easy to obtain the well-crystallized GQDs with 2D morphology. Further control of reaction temperature improves the crystal quality and QY of GQDs. These GQDs with high quality exhibit typical absorption peak for graphene and have intrinsic ultraviolet and blue emissions. Temperature-dependent PL measurements illustrate strong electron-electron scattering and electron-phonon interactions, suggesting a similar temperature behavior of GQDs as inorganic semiconductor quantum dots. By careful analysis of optical properties, we have presented that ultraviolet emission is from the recombination of electron-hole pairs localized in the C–C bonds while the blue one originates from the electron transition of $sp^2$ domains.

## ACKNOWLEDGMENTS

[1]Q. Xiang, J. Yu, and M. Jaroniec, Chem. Soc. Rev. **41**, 782 (2012).
[2]R. R. Nair, P. Blake, A. N. Grigorenko, K. S. Novoselov, T. J. Booth, T. Stauber, N. M. R. Peres, and A. K. Geim, Science **320**, 1308 (2008).
[3]C. Lee, X. Wei, J. W. Kysar, and J. Hone, Science **321**, 385 (2008).
[4]K. S. Novoselov, A. K. Geim, S. V. Morozov, D. Jiang, Y. Zhang, S. V. Dubonos, I. V. Grigorieva, and A. A. Firsov, Science **306**, 666 (2004).
[5]L.-S. Li and X. Yan, J. Phys. Chem. Lett. **1**, 2572 (2010).
[6]L.-L. Li, J. Ji, R. Fei, C.-Z. Wang, Q. Lu, J.-R. Zhang, L.-P. Jiang, and J.-J. Zhu, Adv. Funct. Mater. **22**, 2971 (2012).
[7]K. Nakada, M. Fujita, G. Dresselhaus, and M. S. Dresselhaus, Phys. Rev. B **54**, 17954 (1996).
[8]Y.-W. Son, M. L. Cohen, and S. G. Louie, Phys. Rev. Lett. **97**, 216803 (2006).
[9]V. Barone, O. Hod, and G. E. Scuseria, Nano Lett. **6**, 2748 (2006).
[10]L. Yang, C.-H. Park, Y.-W. Son, M. L. Cohen, and S. G. Louie, Phys. Rev. Lett. **99**, 186801 (2007).

[11]J. Shen, Y. Zhu, X. Yang, J. Zong, J. Zhang, and C. Li, New J. Chem. **36**, 97 (2012).

[12]L. Li, G. Wu, G. Yang, J. Peng, J. Zhao, and J.-J. Zhu, Nanoscale **5**, 4015 (2013).

[13]S. Zhu, J. Zhang, S. Tang, C. Qiao, L. Wang, H. Wang, X. Liu, B. Li, Y. Li, W. Yu, X. Wang, H. Sun, and B. Yang, Adv. Funct. Mater. **22**, 4732 (2012).

[14]F. Liu, M.-H. Jang, H. D. Ha, J.-H. Kim, Y.-H. Cho, and T. S. Seo, Adv. Mater. **25**, 3657 (2013).

[15]L. Wang, S.-J. Zhu, H.-Y. Wang, S.-N. Qu, Y.-L. Zhang, J.-H. Zhang, Q.-D. Chen, H.-L. Xu, W. Han, B. Yang, and H.-B. Sun, ACS Nano **8**, 2541 (2014).

[16]S. Zhu, J. Zhang, C. Qiao, S. Tang, Y. Li, W. Yuan, B. Li, L. Tian, F. Liu, R. Hu, H. Gao, H. Wei, H. Zhang, H. Sun, and B. Yang, Chem. Commun. **47**, 6858 (2011).

[17]Y. Li, Y. Hu, Y. Zhao, G. Shi, L. Deng, Y. Hou, and L. Qu, Adv. Mater. **23**, 776 (2011).

[18]D. Pan, J. Zhang, Z. Li, and M. Wu, Adv. Mater. **22**, 734 (2010).

[19]J. Peng, W. Gao, B. K. Gupta, Z. Liu, R. Romero-Aburto, L. Ge, L. Song, L. B. Alemany, X. Zhan, G. Gao, S. A. Vithayathil, B. A. Kaipparettu, A. A. Marti, T. Hayashi, J.-J. Zhu, and P. M. Ajayan, Nano Lett. **12**, 844 (2012).

[20]L. Lin and S. Zhang, Chem. Commun. **48**, 10177 (2012).

[21]K. P. Loh, Q. Bao, G. Eda, and M. Chhowalla, Nat. Chem. **2**, 1015 (2010).

[22]G. Eda, Y.-Y. Lin, C. Mattevi, H. Yamaguchi, H.-A. Chen, I.-S. Chen, C.-W. Chen, and M. Chhowalla, Adv. Mater. **22**, 505 (2010).

[23]L. Tang, R. Ji, X. Cao, J. Lin, H. Jiang, X. Li, K. S. Teng, C. M. Luk, S. Zeng, J. Hao, and S. P. Lau, ACS Nano **6**, 5102 (2012).

[24]X. Li, S. P. Lau, L. Tang, R. Ji, and P. Yang, Nanoscale **6**, 5323 (2014).

[25]M. Li, W. B. Wu, W. C. Ren, H.-M. Cheng, N. J. Tang, W. Zhong, and Y. W. Du, Appl. Phys. Lett. **101**, 103107 (2012).

[26]Q. Feng, Q. Q. Cao, M. Li, F. C. Liu, N. J. Tang, and Y. W. Du, Appl. Phys. Lett. **102**, 013111 (2013).

[27]F. C. Liu, T. Tang, Q. Feng, M. Li, Y. Liu, N. J. Tang, W. Zhong, and Y. W. Du, J. Appl. Phys. **115**, 164307 (2014).

[28]W. Gu, W. Zhang, X. Li, H. Zhu, J. Wei, Z. Li, Q. Shu, C. Wang, K. Wang, W. Shen, F. Kang, and D. Wu, J. Mater. Chem. **19**, 3367 (2009).

[29]S. M. Seyed-Talebi, J. Beheshtian, and M. Neek-amal, J. Appl. Phys. **114**, 124307 (2013).

[30]S. Kim, S. W. Hwang, M.-K. Kim, D. Y. Shin, D. H. Shin, C. O. Kim, S. B. Yang, J. H. Park, E. Hwang, S.-H. Choi, G. Ko, S. Sim, C. Sone, H. J. Choi, S. Bae, and B. H. Hong, ACS Nano **6**, 8203 (2012).

[31]See supplementary material at http://dx.doi.org/10.1063/1.4904958 for FT-IR spectrum and HRTEM image of GQDs, UV-vis absorption spectra and PL spectra of GQDs obtained at different reaction temperature with different concentrate sulfuric acid.

[32]A. C. Ferrari and J. Robertson, Phys. Rev. B **61**, 14095 (2000).

[33]A. Gupta, G. Chen, P. Joshi, S. Tadigadapa, and P. C. Eklund, Nano Lett. **6**, 2667 (2006).

[34]W. Chen and L. Yan, Nanoscale **2**, 559 (2010).

[35]L. Yang, J. Deslippe, C.-H. Park, M. L. Cohen, and S. G. Louie, Phys. Rev. Lett. **103**, 186802 (2009).

[36]L. Tang, R. Ji, X. Li, G. Bai, C. P. Liu, J. Hao, J. Lin, H. Jiang, K. S. Teng, Z. Yang, and S. P. Lau, ACS Nano **8**, 6312 (2014).

[37]H. He, H. Li, T. Zhang, L. Sun, and Z. Ye, RSC Adv. **4**, 18141 (2014).

[38]T. W. Hagler, K. Pakbaz, K. F. Voss, and A. J. Heeger, Phys. Rev. B **44**, 8652 (1991).

[39]S.-H. Lim, T. G. Bjorklund, and C. J. Bardeen, Chem. Phys. Lett. **342**, 555 (2001).

[40]S. Guha, J. D. Rice, Y. T. Yau, C. M. Martin, M. Chandrasekhar, H. R. Chandrasekhar, R. Guentner, P. Scanduicci de Freitas, and U. Scherf, Phys. Rev. B **67**, 125204 (2003).

[41]X. Wen, A. Sitt, P. Yu, Y.-R. Toh, and J. Tang, Phys. Chem. Chem. Phys. **14**, 3505 (2012).

[42]A. Narayanaswamy, L. F. Feiner, A. Meijerink, and P. J. van der Zaag, ACS Nano **3**, 2539 (2009).

[43]K. P. O'Donnell and X. Chen, Appl. Phys. Lett. **58**, 2924 (1991).

[44]P. Yu, X. M. Wen, Y.-R. Toh, and J. Tang, J. Phys. Chem. C **116**, 25552 (2012).

[45]A. Bostwick, T. Ohta, T. Seyller, K. Horn, and E. Rotenberg, Nat. Phys. **3**, 36 (2007).